

# Local-density-derived semiempirical nonlocal pseudopotentials for InP with applications to large quantum dots

Huaxiang Fu and Alex Zunger

*National Renewable Energy Laboratory, Golden, Colorado 80401*

-Received 5 August 1996!

In the same way that *atomic* calculations have been used previously to extract *bare* ionic pseudopotentials, self-consistent *bulk* calculations can be used to construct *screened* atomic pseudopotentials. We use such a method to construct screened nonlocal atomic pseudopotentials for InP. A series of bulk, local-density-approximation -LDA! calculations are performed on a few InP crystal structures, covering a range of unit-cell volumes, to produce bulk potentials  $V_{\text{LDA}}(\mathbf{G})$ ! By solving a set of linear equations, we extract from these crystalline potentials the corresponding screened *atomic* ‘‘spherical LDA’’ -SLDA! potentials  $v$

such that the wave functions are LDA-like while the band structures, effective masses, and deformation potentials match experiments. Here we apply this “semiempirical pseudopotential method” -SEPM! to both the bulk structure and nanostructures of InP.

The present work differs from our previous work<sup>13</sup> in several aspects:

-i! We develop and apply pseudopotentials for a new material system—bulk InP and InP quantum dots on which numerous experiments have been recently performed,<sup>18–23</sup> but little theoretical work is available. InP dots have been recently synthesized either as strain-induced “self-assembled” particles in metalorganic vapor phase epitaxy,<sup>20,21</sup> or as particles in colloidal solution growth.<sup>22,23</sup> The dot sizes range from 20 to 600 Å. Some interesting phenomena were found, e.g., the evolution of photoluminescence -PL! intensity with pressure,<sup>18</sup> the strong dependence of PL decay time on the photon energy,<sup>19</sup> the blueshift of the PL peak with the photoexcitation power, and band-gap renormalization effects.<sup>20,21</sup> Quantitative analyses of such experiments require a practical and reliable computational tool, which can reproduce excitation energies, wave-function information -e.g., transition probabilities!, effective masses, and deformation potentials. The present method is suitable for such purposes.

-ii! We wish to understand the limitation of the SEPM. The SEPM approach<sup>13</sup> relies on representing the screened solid-state pseudopotential as linear combination of overlapping but *spherical* “site potentials,” and on system-to-system transferability. If such potentials are transferable from one structure to another, their Fourier transforms will lie on a “universal” potential-versus-momentum curve. We have seen previously<sup>13</sup> that both the spherical approximation and the transferability approximation work very well for Si and CdSe. But unlike Si and CdSe, the atomic size difference between In and P is very large, so the directional charge transfer in InP could be significant, raising questions on the suitability of the spherical approximation. Indeed, we find that there is a larger error for InP in the *b*-Sn structure than in the zinc-blende and rocksalt structures. We further find that the asymmetric part of the InP “spherical LDA” -SLDA!

$$V_{\text{LDA}}^{-s}(\mathbf{G}) = \sum_a S^{(a,s)}(\mathbf{G}) v_{\text{SLDA}}^{-a,s}(\mathbf{G}), \quad (3)$$

where  $S^{(a,s)}(\mathbf{G}) = \sum_s V_s^{21}(\mathbf{r}_{a,s}) e^{i\mathbf{G} \cdot \mathbf{r}_{a,s}}$  is the structure factor and  $\mathbf{G}$  is a reciprocal lattice vector. Note that  $v_{\text{SLDA}}^{-a,s}$  is not a free-atom potential, but rather a solid-embedded site potential. The SLDA site potentials can be written conveniently as a symmetric part  $v_{\text{SLDA}}^{-1}(\mathbf{G})$  and an asymmetric part  $v_{\text{SLDA}}^{-2}(\mathbf{G})$ :

$$v_{\text{SLDA}}^{-1}(\mathbf{G}) \pm v_{\text{SLDA}}^{-\text{In}}(\mathbf{G})$$

ued at the shortest bulk  $\mathbf{G}$  vectors. This deviation of  $v_{\text{SLDA}}^{(2)}(\|\mathbf{G}\|)$  from a universal curve did not occur in Si (for which  $v_{\text{SLDA}}^{(2)}(\|\mathbf{G}\|) \neq 0$ ) or in CdSe (see Fig. 1 in Ref. 13). We also observe that this nontransferability error is mainly reflected in the asymmetric potential  $v_{\text{SLDA}}^{(2)}(\|\mathbf{G}\|)$ , while the symmetric potentials  $v$

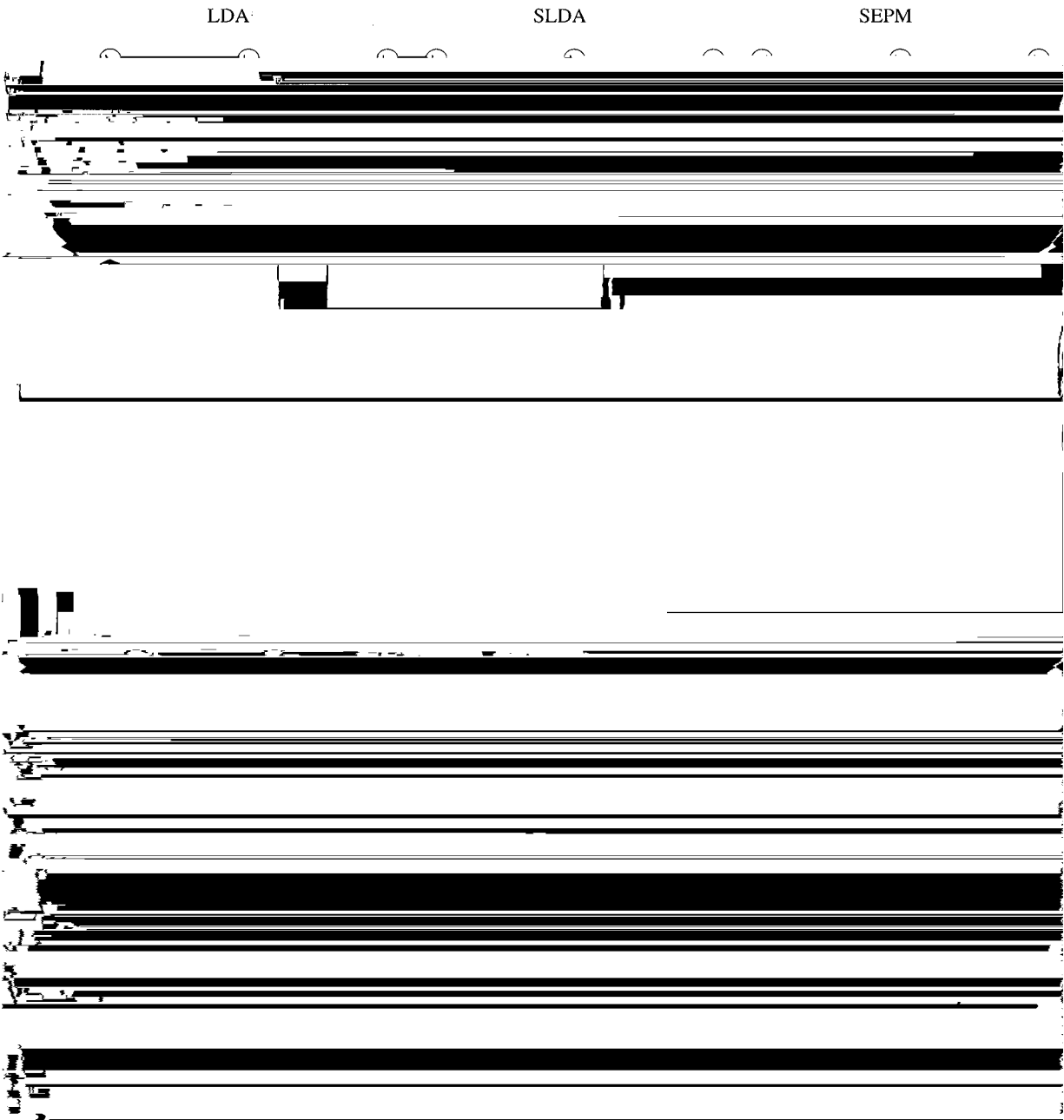


FIG. 3. Contour plots of wave-function squares on the  $-110$  plane for the  $G_{15v}$ ,  $G_{1c}$ ,  $X_{5v}$ , and  $X_{1c}$  states in zinc-blende InP ( $a=5.1101$  a.u.) as calculated by using LDA, SLDA, and SEPM potentials. The LDA and SLDA results are obtained using kinetic cutoff energy  $E_{\text{cut}}=25$  Ry, and the SEPM results are obtained using  $E_{\text{cut}}=6.8$  Ry and the Gaussian correction (Appendix B).

averaged errors between the LDA and the SLDA results are 0.07 and 0.02 eV for the lowest eight bands in zinc-blende and rocksalt InP, respectively. In the metallic  $b$ -Sn form, the error is larger: 0.35 eV for the first and fifth bands and 0.1 eV for other bands. In order to find the reason for this relatively large error, we intentionally let the fitted curve in Fig. 1-b) pass through the  $b$ -Sn data points. Application of this potential to study the band structure will result in error reflecting only the spherical approximation. We find that in the  $b$ -Sn structure the spherical approximation error is about 0.15 eV and the nontransferability error is 0.20 eV for the first and fifth bands. We attribute the relatively larger error for  $b$ -Sn structure to the large difference in the sizes of the In and P atoms, and to the low symmetry of the  $b$ -Sn structure.

We find that the LDA wave functions are also accurately reproduced by our fitted SLDA potentials. As an example, Fig. 3 compares the contour plots of the wave-function squares for the  $G_{15v}$ ,  $G_{1c}$ ,  $X_{5v}$ , and  $X_{1c}$  states of zinc-blende InP as calculated from the LDA and from the fitted SLDA potentials. The agreement is excellent: the LDA versus SLDA wave-function overlap is larger than 99.9%.

The first three columns in Table I<sup>29-41</sup> compare zinc-blende InP band energies, effective masses, and deformation potentials obtained from LDA and SLDA calculations, showing good agreement.

The good agreement between LDA and SLDA calculations persists after we reduce the kinetic cutoff energy from 25 to 6.8 Ry, while compensating for the reduced basis by

using the ‘‘Gaussian correction’’ -GC! method<sup>13</sup> as described in Appendix B and in Fig. 4. The reduction of the kinetic energy cut-off can reduce significantly the computational effort for quantum nanostructures.

### B. SEPM potentials and their performance for bulk InP

In the next step, we apply linear changes to the curve-fitted potentials  $v_{\text{SLDA}}^{\text{G}}$ . @.e., we only change the coefficients  $c_i$  in Eq. 6!# so as to fit their bulk eigenvalues to the experimentally observed excitations. The obtained potential is called the SEPM potential. The required changes in the potentials are found to be small, and therefore the changes in the wave functions relative to the LDA calculation are also small.

Table I compares the band energies, effective masses, and deformation potentials obtained by using the SLDA potential and the empirically corrected potential -SEPM!. In this table, the pertinent experimental results are included for comparison. We see that the SEPM achieves good accord with the pertinent experimental quantities, including the band structures at G, X, and L points, the effective masses and deformation potentials. The SEPM band structures of InP in zincblende structures are compared in Fig. 5 with the SLDA band structures. We see that, except for the upshifts of the conduction bands, the main features and trends of the whole

SEPM band structures follow those of the SLDA. The wavefunction squares of SEPM calculations for some bulk states are illustrated in Fig. 3, showing good agreement with LDA and SLDA results.

### C. Effects of removing the LDA error

The G-space SEPM potential and the shift  $Dv = v_{\text{SEPM}}^{\text{G}} - v_{\text{SLDA}}^{\text{G}}$ , needed to remove the LDA error in the band structures, are shown in Fig. 6, while Fig. 7 shows  $v_{\text{SEPM}}^{\text{G}}$  and  $Dv$

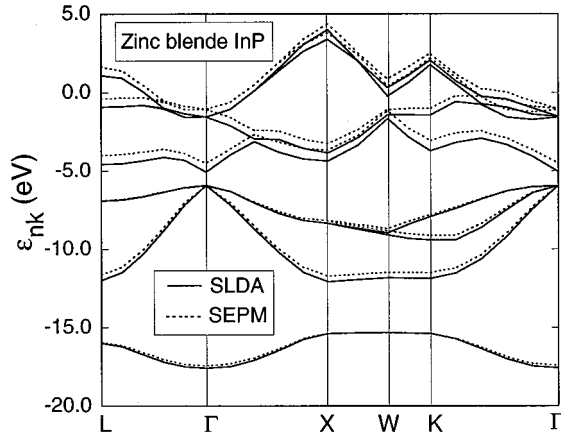


FIG. 5. The zinc-blende InP band structure calculated from SEPM -dotted lines! and from SLDA potentials -solid lines!. The lattice constant is  $a \approx 11.01$  a.u. Both the SEPM and the SLDA band energies are given in absolute values. Since the VBM positions are very close to each other for LDA and SLDA bands, this figure shows that most of the LDA error is in the conduction bands.

formed from the  $s$  orbitals of the two atoms! is mainly determined by the atomic energy level of the In  $s$  orbital. The increase of the SEPM potential relative to the SLDA potential in the In core region will push up the atomic energy level

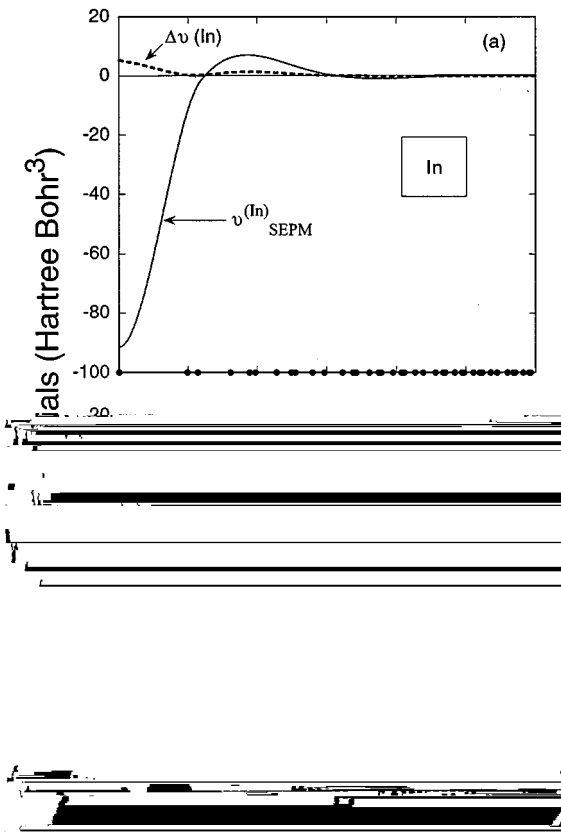


FIG. 6. The semiempirical atomic potentials  $v_{\text{SEPM}}^{\text{al}}$  -solid lines! and the shift  $D \approx v_{\text{SEPM}}^{\text{al}} - v_{\text{SEPM}}^{\text{sl}}$  -dotted lines! in  $\mathbf{G}$  space: -a! for In; -b! for P. Dots on the axis indicate zinc-blende reciprocal lattice-vector lengths for bulk InP.

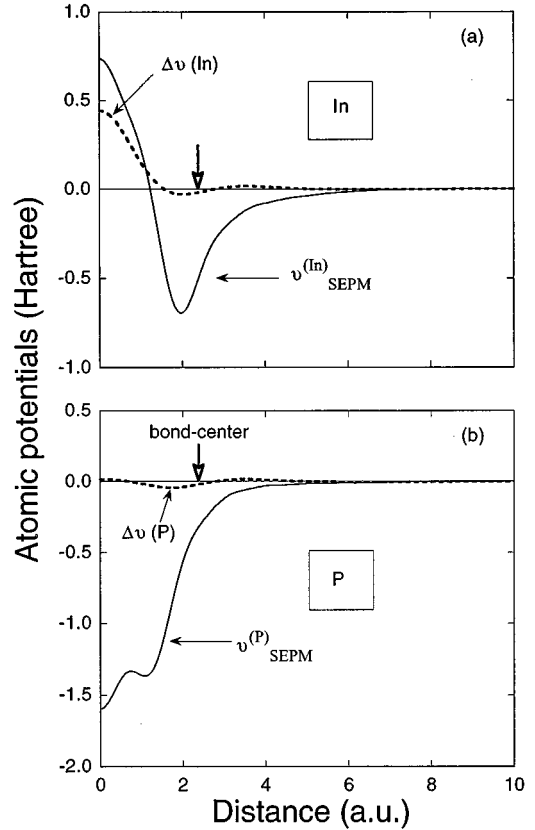


FIG. 7. The semiempirical atomic potentials  $v_{\text{SEPM}}^{\text{al}}$  -in solid lines! and the shift  $D$

of the In  $s$  orbital, consequently raising the lowest conduction band. Due to the orthogonalization constraint, the higher conduction bands will also be pushed up as shown in Fig. 5. The valence bands bear only little change since the  $p$  orbital energy is not affected by shifting the In potential near the origin. Furthermore, since the potentials near the In-P bond center do not change significantly, the In-P interaction will not change much. This suggests that the wave function will not change too much either. This is borne out by the similarity of SEPM and LDA wave functions shown in Fig. 3. The fact that the error in SLDA potential is mostly in the atomic core region and is different for  $s$  and  $p$  valence electrons suggests that one could improve the SEPM fit by treating the nonlocal part of the pseudopotential also as a parametrized function. At this stage, however, we prefer not to introduce additional fitting functions.

(ii) *Energy location of the LDA error:* Figure 5 gives the SEPM and SLDA bands of zinc-blende InP on an absolute scale -i.e., the VBM's are not aligned!. The comparison of SEPM band structures relative to SLDA results shows that the main effect of the removal of LDA error is to move the conduction bands up while the valence bands do not change much. This situation is similar to what was found in more elaborated  $GW$  calculations.<sup>42</sup>

#### D. Effect of the potential slope at G50 on nanostructures

So far, our discussion has centered on bulk materials. Application of SEPM potentials to quantum nanostructures

-which contain reciprocal lattice vectors that are absent in the bulk! requires that the potentials should be flat near  $\mathbf{G}_5$



$$u_a \approx u_a^0 \exp(-2|\mathbf{r} - \mathbf{R}|/r_a^0), \quad -10!$$

where  $\mathbf{R}$  is the spatial position of the passivating atom. The parameters  $u_a^0, r_a^0$  are selected so as to fit the calculated surface density of states of planar InP surfaces to LDA results or to photoemission data for surfaces.<sup>47</sup> This procedure was described in Ref. 11 for Si. Here we illustrate the electronic structure of InP quantum dots using the typical values: For the InP-110! surface,  $u_a^0 \approx 23.5$  hartrees and  $r_a^0 \approx 0.9$  a.u. for surface In, and  $u_a^0 \approx 22.0$  hartrees and  $r_a^0 \approx 1.0$  a.u. for surface P. For the InP-100! surface,  $u_a^0 \approx 21.5$  hartrees and  $r_a^0 \approx 1.4$  a.u. for surface In, and  $u_a^0 \approx 20.5$  hartrees and  $r_a^0 \approx 1.5$  a.u. for surface P. These values produce a band gap free of surface states for all the InP-110! and InP-001! films.<sup>47</sup> We point out that, after removing the surface states out of the gap, the band-edge energy levels of dots are not sensitive to the passivating potentials. We will return to this point later.

In order to solve the Schrödinger equation with many atoms, we use the folded spectrum and conjugate gradient methods,<sup>11</sup> allowing us to find the energy levels and wave functions of the CBM and VBM states of dots. The calculated band gaps for these dots are illustrated in Fig. 9-a! while the VBM and CBM energy levels of dots are shown in Fig. 9-b!. For comparison, the available experimental data from absorption spectrum<sup>22</sup> and PL measurements<sup>23</sup> are also shown in Fig. 9-a!. The experimental values are converted to one-electron band gaps by subtracting the electron-hole Coulomb energy calculated from  $E_c \approx 23.572/\epsilon D$  -Ref. 48!. Here,  $E_c$  and the size  $D$  are both given in atomic units, and the static dielectric constant  $\epsilon$  of InP is<sup>49</sup> 12.4. Figure 9-a! shows that the theoretical one-electron gaps are in good agreement with the experimental measurements. The quantum size effects on both the CBM and the VBM of dots are obvious in Fig. 9-b!. Note that the energy levels in Fig. 9-b! are absolute values since our SEPM potentials are obtained by fitting the work function. Therefore, we can discuss the size effect separately for the VBM and the CBM of dots. We fitted our calculated band gaps  $E_g$  in units of eV! versus the size of InP dots  $D$  in units of Å! as

$$E_g \approx 1.45 + 37.295/D^n, \quad n \approx 1.16. \quad -11!$$

include here explicit surface effects. For bare -unpassivated! dots, the atoms at the surface will most likely reconstruct. Here we model, instead, dots grown by self-assembled method<sup>20,21</sup> or by colloidal solution.<sup>22,23</sup> In both cases, the atoms at the surface are passivated chemically either by another semiconductor<sup>20,21</sup> or by organic molecules,<sup>22,23</sup> so the surface is, most likely, unreconstructed. Generally, the surface conditions of dots are different for differently prepared samples. However, based on the measurements of PL lifetime and PL efficiency, it is found that the emission originates mostly from dot-interior -“bulklike”! states, not from surface states. In recent experiments for InP dots, organic compounds and HF solution are used to passivate and etch the surface.<sup>22,23</sup> In these experiments, the passivation effect of organic compounds and HF at the InP dot surface is quite similar to attaching an electrostatic potential to the surface dangling bond. We thus simulate the actual passivation in dots by attaching the following fictitious pseudopotential to In-like and P-like dangling bonds:

This analytic equation is described by the dashed line in Fig. 9-a!. Not surprisingly, the value  $n \approx 1.16$  from our atomistic calculation is very different from that found in classic effective-mass theory of  $n \approx 2.0$ .

In order to investigate the natures of the VBM and CBM of dots, we have calculated the planar-averaged wave-function square  $\overline{|C_m|^2}$  along certain directions, where  $m$  is the energy-level index. The planar-averaged wave-function square  $\overline{|C_m|^2}(x)$  along the  $x$  direction and  $\overline{|C_m|^2}(z)$  along the  $z$  direction are defined as

$$\overline{|C_m|^2}(x) \approx \frac{1}{S_{yz}} \int \overline{|C_m(\mathbf{r})|^2} dy dz, \quad -12!$$

$$\overline{|C_m|^2}(z)!$$

wave bases. This is illustrated here for the band gaps of InP

lar to the  $z$  axis, respectively. For the InP dots considered here, the  $x$ ,  $y$ , and  $z$  axes are along  $\bar{1}10$ ,  $\bar{1}\bar{1}0$ , and  $\bar{0}01$  directions of InP zinc-blende structure, respectively. The  $x$  and  $y$  directions are equivalent for the dots considered here. Figures 10-a) and 10-b) give, respectively, the planar-averaged wave-function squares  $\overline{\|C_m\|^2}(x)$  and  $\overline{\|C_m\|^2}(z)$  for the dot with 712 atoms. In this figure, symbols along the horizontal axis indicate atomic-layer positions in the dot. From Fig. 10, we can see that the wave functions of both the CBM and VBM are mostly distributed in the interior of dot, with but little amplitude at the dot surface. For such “dot-interior” states, changes in the passivation potential -e.g., different saturation species- cannot shift these energy levels significantly. A similar situation is found in experiments.<sup>22,23</sup>

In summary, we derive the semiempirical pseudopotentials for InP from *ab initio* LDA pseudopotential calculations. The obtained SEPM potentials reproduce accurately the LDA wave functions and the experimentally observed band structures, effective mass, and deformation potential. Since it is soft, the SEPM potential can be used efficiently in large-scale quantum nanostructure calculations using plane-

$$\tilde{v}_{\text{SLDA}}^{-1!} \sim r!5@a_1$$

- <sup>28</sup>D. R. Hamann, M. Schluter, and C. Chiang, Phys. Rev. Lett. **43**, 1494 -1979!.
- <sup>29</sup>J. van Laar, A. Huijser, and T. L. van Rooy, J. Vac. Sci. Technol. **14**, 894 -1977!.
- <sup>30</sup>L. Ley and R. A. Pollak, Phys. Rev. B **9**, 600 -1974!.
- <sup>31</sup>Z. Hang, H. Shen, and F. H. Pollak, Solid State Commun. **36**, 15 -1990!.
- <sup>32</sup>P. Lautenschlager, M. Garriga, and M. Cardona, Phys. Rev. B **36**, 4813 -1987!.
- <sup>33</sup>S. W. Tozer, D. J. Wolford, J. A. Bradley, D. Bour, and G. B. Stringfellow, *Proceedings of the 19th ICPS, Warsaw, Poland*, edited by W. Zawadski -Institute of Physics, Polish Academy of Sciences, 1988!, p. 881.
- <sup>34</sup>L. W. James, J. P. Van Dyke, F. Herman, and D. M. Chang, Phys. Rev. B **1**, 3988 -1970!.
- <sup>35</sup>P. Rochon and E. Fortin, Phys. Rev. B **12**, 5803 -1975!.
- <sup>36</sup>J. M. Chamberlain, J. Phys. C **4**, L38 -1971!.
- <sup>37</sup>J. Leotin, R. Barbaste, S. Askenazy, M. S. Skolnick, R. A. Stradling, and J. Tuchendler, Solid State Commun. **15**, 693 -1974!.